POLITECNICO
MILANO 1863

RE.PUBLIC@POLIMI
Research Publications at Politecnico di Milano

Post-Print

This is the accepted version of:

M. D'ottavio, A. Krasnobrizha, E. Valot, O. Polit, R. Vescovini, L. Dozio
Dynamic Response of Viscoelastic Multiple-Core Sandwich Structures
Journal of Sound and Vibration, Vol. 491, 2021, 115753 (17 pages)
doi:10.1016/j.jsv.2020.115753

The final publication is available at https://doi.org/10.1016/j.jsv.2020.115753

Access to the published version may require subscription.

When citing this work, cite the original published paper.

© 2021. This manuscript version is made available under the CC-BY-NC-ND 4.0 license
http://creativecommons.org/licenses/by-nc-nd/4.0/

Permanent link to this version
http://hdl.handle.net/11311/1146913

*Manuscript

Dynamic response of viscoelastic multiple-core sandwich structures

M. D'Ottavio[a,1], A. Krasnobrizha[a], E. Valot[a], O. Polit[a], R. Vescovini[b], L. Dozio[b]

[a]*Laboratoire Energétique Mécanique Electromagnétisme, Université Paris Nanterre*
50, rue de Sèvres, 92410 Ville d'Avray, France
[b]*Dipartimento di Scienze e Tecnologie Aerospaziali, Politecnico di Milano*
Via La Masa 34, 20156 Milano, Italy

Abstract

This work focuses on the free and forced vibrations of sandwich beams and plates hosting an arbitrary number of damping cores. A fractional derivatives Zener-type model is adopted for representing the frequency-dependent viscoelastic behaviour, along with conventional series developments. The structural models are formulated within an established variable kinematics approach, which enables to investigate the role of specific assumptions and to identify the most accurate model at a least number of degrees of freedom. Approximate solutions are found by a computationally efficient Ritz method that allows to take into account any type of boundary conditions. Modal loss factors and damped eigenfrequencies are obtained from a complex eigenvalue problem, for which a modal strain energy approach or a complex eigensolution can be employed. Frequency responses can be computed by a direct approach or by elementary modal projection algorithms. Results are reported for conventional and innovative sandwich configurations. Different modelling and solution strategies are compared and the role of transverse normal deformation of the mechanically weak viscoelastic plies is particularly emphasised.

Keywords: Viscoelastic damping, Variable kinematics, Ritz method, Fractional derivatives model, Multiple-core sandwich

1. Introduction

Viscoelastic materials (VEM) have been proven to be an attractive means for improving structural vibration damping, which is of particular relevance for noise attenuation [1] but also for enhancing dynamic stability, impact resistance and fatigue life. These materials are particularly effective when implemented as constrained layers, a configuration that can be realised within either

[1]Corresponding author. Dr.-Ing. Michele D'Ottavio, Email: mdottavi@parisnanterre.fr

passive or hybrid vibration control approaches [2]. In order to properly account for the damping performances in the design phase, appropriate modelling techniques are required. The inherent complexity of both, the underlying physical mechanisms characterising the viscoelastic behaviour and the resulting structural response, has stimulated an important research effort. In the following, attention is restricted to linear and non-ageing VEM in an isothermal setting, although it is worth recalling that the operating temperature is an important parameter of the viscoelastic damping properties [3]. Furthermore, since the present work is focused on the harmonic response, i.e., free-vibration and frequency response, the attention will be mainly given to structural models inscribed within the conventional Complex Modulus Approach (CMA).

The frequency-dependent dynamic modulus and loss factor of the most employed VEM, such as elastomers, has been of main concern. The Golla-Hughes-McTavish (GHM) [4] and the Anelastic Displacement Field (ADF) [5] approaches introduce internal variables for describing the viscoelastic behaviour in terms of generalised rheological models, which represent the dissipation function as a sum of individual relaxation processes, such as the generalised Maxwell or Kelvin-Voigt models. These integral approaches are quite compatible with the conventional Finite Element (FE) discretisation of the equation of motion in time domain, but can also be employed in the frequency domain within the CMA. However, an accurate representation of weakly frequency-dependent materials requires a large number of parameters. A convenient representation of this class of materials relies on a constitutive law described by fractional derivatives (FD) [6–8], an approach that has several appealing features as it is causal, mechanically justified and thermodynamically sound, and it allows to describe the material behaviour over a broad frequency range with a relatively small number of parameters, typically four or five [9, 10]. Despite the evaluation of differential operators of fractional order comes along with a certain computational burden [11], the use of FD models in the frequency domain within the CMA is straightforward.

From the computational point of view, the determination of modal loss factors and damped eigenmodes of structures with embedded frequency-dependent materials amounts to solve complex and nonlinear eigenvalue problems. Several numerical techniques have been devised for an efficient though accurate solution of this challenging algebraic problem: the nonlinear Arnoldi method [12], the Order-Reduction-Iteration approach [13], or methods based on an asymptotic expansion of the eigensolution [14, 15]. The so-called Direct Frequency Response (DFR) can be alternatively used, from which the structural damping can be extracted from the resonant peaks [16]. The Modal Strain

Energy (MSE) approach reduces the computational cost of the complex eigenvalue problem by using the undamped mode shapes for estimating the energy contribution of the viscoelastic damping and thus the loss factors [17, 18]. This approximation appears particularly meaningful for lightly damped structures in which the damped modes differ only marginally from the undamped ones. An Iterative MSE (IMSE) scheme allows to extend the MSE approach to frequency-dependent viscoelasticity [19, 20]. Several algorithms improve the accuracy of the MSE approach upon retaining the imaginary part of the eigenmodes, see, e.g., [2]. A comprehensive numerical assessment of modal projection algorithms can be found in [21].

From the structural point of view, the constrained layer configuration is a sandwich construction, in which the VEM layer acts as the soft core placed amid the basis structure and a stiff constraining layer. In such a configuration, the flexural vibrations of the basis structure induce a transverse shear strain of the viscoelastic material, which in turn drives a broadband energy dissipation [22, 23]. A large variety of modelling approaches have been proposed for predicting the dynamic response of these structures at a less effort, either in terms of analytical treatments or of computational cost. This aspect is of particular relevance in the framework of optimisation studies and by keeping in mind the inherent nonlinearity of frequency-dependent viscoelasticity.

Within classical FE discretisation techniques, the elastic skins are usually discretised using structural elements (beam/plate/shell), while solid elements are used for the VEM layer [24]. In order to reduce the modelling and computational burden associated with the use of solid elements for thin VEM layers, Rouleau *et al.* have developed viscoelastic interface elements that can be connected with standard solid elements available in commercial FE packages [25], while Kpeky *et al.* proposed models entirely based on solid-shell elements [26].

Many *ad-hoc* structural models have been proposed in the framework of dedicated analytical or numerical developments and the following literature review has not the aim of being exhaustive. Three different modelling approaches can be distinguished for multilayered composite structures as Equivalent Single Layer (ESL), Layer-Wise (LW), and ZigZag approaches [27–29]. In an ESL approach, the whole composite stack is homogenised and its behaviour described by a number of unknowns that is independent of the number of physical plies, whereas in a LW approach, each ply is described by a dedicated set of unknown functions. Pertain to the ESL models the well known Classical Lamination Theory (CLT), which relies on Kirchhoff-Love assumptions and neglects the transverse shear deformation, and the First-order Shear Deformation Theory (FSDT), which relies

on Reissner-Mindlin assumptions and retains a transverse shear deformation that is constant across the thickness. Refinements of these classical models can be classified as High-order Shear Deformation Theories (HSDT) and High-order Shear and Normal Deformation Theories (HSNDT); theories pertaining to this latter group retain the transverse normal stress and employ the full 3D constitutive law. A ZigZag model can be constructed starting from a LW model and making the number of unknowns independent from the number of plies through the enforcement of physically meaningful conditions at the interfaces, i.e., the interlaminar C^0-continuity of the displacement and transverse stress fields, see, e.g., the comprehensive overview [30] and the general procedure developed in [31]. Alternatively, so-called ZigZag-Functions can be simply superposed to an ESL displacement field [32]. When dealing with sandwich structures, an ESL approach is known to be inaccurate because it is not capable to account for the strong mismatch between the stiff skins and the soft core [33, 34]. Therefore, various LW and ZigZag models have been proposed for viscoelastic sandwich structures, as discussed in the following.

Within a LW description, the simplest models rely on the fundamental assumption of a "weak" core that does not carry any axial stress and simply transfers the bending stresses of the stiff skins by means of a uniform transverse shear stress [22, 35–39]. However, the most frequently used models nowadays include the axial stresses in the core and the bending stiffness of the skins, i.e., by adopting CLT for the skins and FSDT for the core, see, e.g., [40–46]. Cupiał and Nizoł proposed a critical evaluation of the simplifying assumption of nil transverse shear stress in the elastic skins [47]. Examples of LW models employing FSDT for all layers, elastic and VEM, can be found in [48–50]. In order to improve the transverse shear strain that drives the viscoelastic damping, HSDT have been used for the VEM layer, see e.g., [51–53]. It is worth highlighting that, according to [53], enforcing the interlaminar continuity of the transverse shear stresses does not substantially improve the vibration response of the viscoelastic sandwich.

In order to reduce the number of degrees of freedom (dof) with respect to LW approaches, ZigZag models for sandwich structures with VEM cores have been proposed, e.g., in [54–57] for beams and in [58] for plates.

All the aforementioned models discard the transverse normal strain energy contribution, which, however, can contribute substantially to the viscoelastic energy dissipation depending on the vibration mode of the structure [23]. A more limited number of works consider the so-called transverse compressional damping along with the transverse shear damping, see, e.g., [59, 60]. Ref. [60] is

of particular relevance as it employs a LW description for the sandwich structure, in which CLT is used for modelling the skins and variable kinematics can be adopted for the VEM core by referring to polynomial expansions of different orders for the in-plane and transverse displacements. Variable kinematics approaches are very useful for assessing the accuracy of different models, which is known to be highly problem-dependent [61].

The most established variable kinematics approach has been systematically developed by Carrera [62]. By virtue of a compact index notation, the so-called Carrera Unified Formulation (CUF) enables the implementation in a unique software of structural models ranging from the most constrained CLT and FSDT up to quasi-3D models, including ESL, LW as well as ZigZag models based on HSDT or HSNDT and MZZF. CUF has been formally generalised to allow different expansion orders and descriptions to be used for individual displacement components (Generalized Unified Formulation, GUF) [63] as well as for groups of plies, the *sublaminates* (Sublaminate Generalized Unified Formulation, SGUF) [64]. The application of CUF to composite structures including VEM layers can be found in [65–69].

This paper presents for the first time the extension of the SGUF approach to composite sandwich with frequency-dependent VEM layers. The partial differential equations associated to the variable kinematics plate models are solved in weak form by a highly efficient Ritz method [70]. The SGUF-Ritz approach has already demonstrated its versatility and accuracy in the static, free-vibration and stability analysis of sandwich plates and shells [71–74]. In particular, the present Ritz solution has proven to converge rapidly even in presence of highly anisotropic structures and is capable of handling any type of boundary conditions [75].

2. Viscoelastic models in CMA

The time-dependent constitutive law of a viscoelastic material (VEM) is expressed in the frequency domain through a Fourier transform, which yields the following definition of a complex modulus:

$$E^*(\mathrm{i}\omega) = E'(\omega) + \mathrm{i}\, E''(\omega) = E'(\omega)\left[1 + \mathrm{i}\,\eta(\omega)\right] \tag{1}$$

Throughout the paper, complex variables are denoted by an asterisk and $\mathrm{i} = \sqrt{-1}$ is the imaginary unit. In Eq. (1), E' is the dynamic or storage modulus and E'' is the loss modulus. The ratio between

the loss and storage modulus measures the material damping through the loss factor η :

$$\eta(\omega) = \frac{E''(\omega)}{E'(\omega)} \tag{2}$$

2.1. Anelastic Displacement Fields model

Following Lesieutre and Bianchini [5], a frequency-dependent viscoelastic material can be described within the CMA as a series of $j = 1, 2 \ldots n$ Kelvin-Voigt elements and an elastic spring according to the following expression:

$$G^*(\omega) = G_0 \left(1 + \sum_{j=1}^{n} \frac{\Delta_j \, \omega}{\omega - \mathrm{i}\, \Omega_j} \right) \tag{3}$$

where $G_0 = G^*(\omega \to 0)$ is the "relaxed" or static modulus of elasticity, and $1/\Omega_j$ and Δ_j are the relaxation time and strength, respectively, of the j^{th} Kelvin-Voigt element. At very high frequencies, the VEM response is purely elastic and is characterised by the high-frequency limit of the dynamic modulus ("unrelaxed" modulus) $G_\infty = G^*(\omega \to \infty) = G_0(1 + \sum_j \Delta_j)$.

2.2. Fractional derivatives Zener model

The fractional derivatives Zener (FDZ) model employed in this work describes the VEM behaviour in the frequency domain by means of the following expression that involves only 4 parameters [9]

$$G^*(\omega) = \frac{G_0 + G_\infty (\mathrm{i}\, \omega\, \tau)^\alpha}{1 + (\mathrm{i}\, \omega\, \tau)^\alpha} \tag{4}$$

As in Eq. (3), G_0 is the static modulus and $G_\infty = G^*(\omega \to \infty)$ is the unrelaxed modulus, while α is the fractional order of derivatives and τ the relaxation time. In order to respect the second principle of thermodynamics, the following conditions must hold [8]:

$$G_\infty > G_0 > 0, \quad \tau > 0, \quad \text{and} \quad 0 < \alpha \leq 1 \tag{5}$$

2.3. Identification of viscoelastic material parameters

A procedure is described in the following, which allows to identify the FDZ model parameters characterising the frequency-dependent behaviour of a VEM. In particular, the procedure is applied to 2 materials with different data sources, namely the 3M ISD112 polymer, that has been often described in terms of ADF series expansions [5, 19], and the Deltane 350, for which FDZ models have been identified from an experimental master curve [76, 77].

Starting from a reference curve describing the frequency-dependent complex modulus, which may be defined by an ADF model or from other experimentally collected data, the parameters of the FDZ model are determined employing an inverse optimisation procedure whose objective function is the mean square error of the storage and loss moduli G' and G'' over the considered frequency range. A 4-dimensional optimisation problem is thus formulated, whose unknown parameters are G_0, G_∞, τ and α under the constraints given in Eq. (5). It is noticed that the static and unrelaxed moduli G_0 and G_∞ can be uniquely determined within a least-square method once the parameters α and τ are fixed. Several optimisation algorithms have been investigated for the identification, and it has been found that the meta-heuristic Particle Swarm Optimisation (PSO) method [78] provided the most accurate results in a robust manner, taking into account the very different orders of magnitude of the involved parameters and the slightly oscillating nature of the globally convex objective function. A population of 10 particles are employed to solve the problem, which is considered to be converged when the tolerance value of 10^{-6} is reached for the objective function for 10 consecutive iterations. For the applications discussed in this paper, convergence could be generally achieved within a maximum of 70 iterations.

For the 3M ISD112 at 27°C, Lesieutre and Bianchini provided an experimental identification of the ADF parameters related to a series expansion involving $n = 1, 3$ and 5 Kelvin-Voigt elements [5]. The description given by Eq. (3) with $n = 5$ was shown to very well match the experimental response over the frequency range 8 – 8000 Hz. An ADF model with $n = 3$ has been independently identified over the frequency range 20 – 5000 Hz by Trindade *et al.* [19]. The present identification of the FDZ parameters is carried out starting from the ADF models in [5] with $n = 5$ (ADF–5) and with $n = 3$ (ADF–3). The objective function is defined for both cases over two different frequency ranges, namely the FR1 8 – 8000 Hz and the FR2 20 – 5000 Hz. The relaxed modulus G_0 has the same meaning in the FDZ and ADF models and has been here considered as a fixed value, which reduces the optimisation problem to a 3-dimensional one. It has been found that more accurate optimisation results could be obtained by letting G_∞ free to be identified concurrently with α and τ. The numerical values for the FDZ model parameters obtained from the identification are reported in Tab. 1. The corresponding frequency-dependent storage modulus and loss factor are given in Fig. 1 for the ADF–5 and ADF–3 case. The FDZ models identified from the ADF–5 over the two frequency ranges provide very similar, smooth curves that fit well the reference. Also the FDZ models obtained from the ADF–3 model yield smooth curves, however, some discrepancies are

Model	Freq. range	G_0 [MPa]	G_∞ [MPa]	τ [μs]	α
ADF–5	FR1	0.462	152.76	0.522	0.675
	FR2	0.462	171.39	0.444	0.675
ADF–3	FR1	0.493	150.70	0.646	0.691
	FR2	0.493	180.96	0.356	0.674

Table 1: ISD112 at 27°C: FDZ model parameters identified from the ADF models of [5] with $n = 5$ and $n = 3$.

visible in particular for the loss factor due to the slightly oscillating behaviour displayed by the ADF model. Moreover, the curves obtained over the two frequency ranges FR1 and FR2 differ in a more visible manner from each other compared to the curves identified starting from the ADF–5 model.

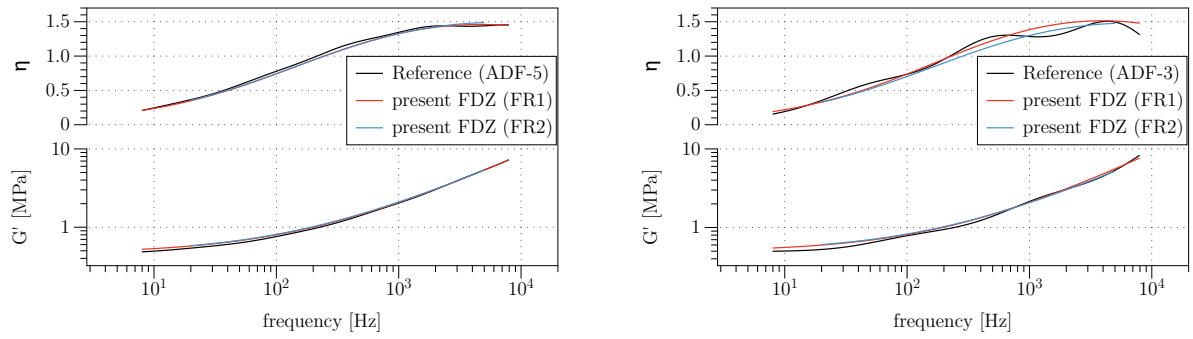

Figure 1: Frequency-dependent storage modulus and loss factor for ISD112: Reference [5] and FDZ curves identified over the frequency ranges FR1 and FR2 from ADF–5 model (left) and ADF–3 model (right).

For the Deltane 350, the identification is carried out starting from the master curve at 12°C reported in [76]. In this case, all four FDZ material parameters are optimised, 40 particles are thus used in the PSO algorithm. Table 2 lists the FDZ parameters obtained by the present identification along with 3 different sets reported in [76, 77]: the set "FDZ-anlt", whose parameters have been analytically estimated by Rouleau [76] according to [11], and the two sets "FDZ-exp1" and "FDZ-exp2" identified from the experimental master curve [76, 77]. The frequency-dependent storage modulus and loss factor of the resulting 4 FDZ models are graphically compared in Fig. 2, in which the reference curve obtained upon digitalisation of the master curve of the manufacturer is also given. One can notice that the analytical estimate of the FDZ parameters may yield to rather inaccurate results, while a reasonable agreement is found for the present FDZ and the FDZ-exp2

Model	G_0 [MPa]	G_∞ [GPa]	τ [μs]	α
FDZ-anlt [76]	1.40	0.54	0.52	0.59
FDZ-exp1 [76]	1.60	0.37	0.69	0.63
FDZ-exp2 [77]	1.88	0.78	0.15	0.50
Present	1.90	0.37	0.56	0.51

Table 2: FDZ model parameters for Deltane 350 at 12°C.

models, whose parameters are identified directly from the experimental curves.

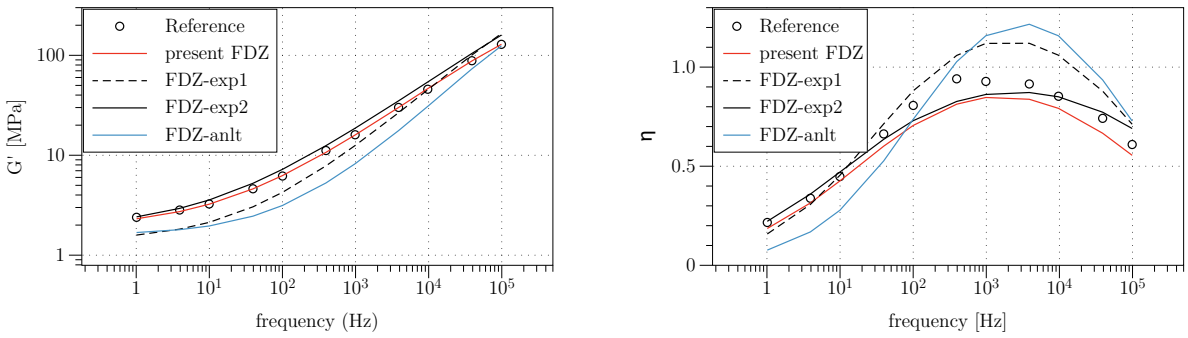

Figure 2: Frequency-dependent storage modulus (left) and loss factor (right) for Deltane 350: Reference curves and FDZ models.

3. Derivation of the governing equations

3.1. Description of the geometry

Let a composite plate occupy the volume $V = \Omega \times \left[-\frac{h}{2} \leq x_3 \leq \frac{h}{2}\right]$, with h denoting the uniform thickness and $\Omega = [0, L_1] \times [0, L_2]$ the reference surface on the $(x_1, x_2)-$plane. Let further be the plate composed of $p = 1, 2, \ldots N_p$ perfectly bonded and homogeneous plies, each of thickness h_p, stacked along the thickness direction $x_3 \equiv z$. As illustrated in Fig. 3, the SGUF approach relies on the subdivision of the composite stack into $k = 1, 2, \ldots N_k$ sublaminates, each of uniform thickness h_k and composed of N_p^k adjacent plies. In the following, quantities related to the ply p of the sublaminate k will be indicated by $()^{p,k}$, p indicating the ply index and k the sublaminate index. Ply- and sublaminate-specific coordinates are introduced as $z_p \in \left[-\frac{h_p}{2}, \frac{h_p}{2}\right]$ and $z_k \in \left[-\frac{h_k}{2}, \frac{h_k}{2}\right]$, respectively. The following dimensionless coordinates are thus defined as

$$\zeta_p = \frac{2z_p}{h_p}; \quad \zeta_k = \frac{2z_k}{h_k} \tag{6a}$$

where the following relation holds

$$\zeta_p = \frac{h_k}{h_p}\zeta_k + \frac{2}{h_p}\left(z_{0k} - z_{0p}\right) \tag{6b}$$

with z_{0p} and z_{0k} denoting the coordinates of the midplanes of the ply and sublaminate, respectively.

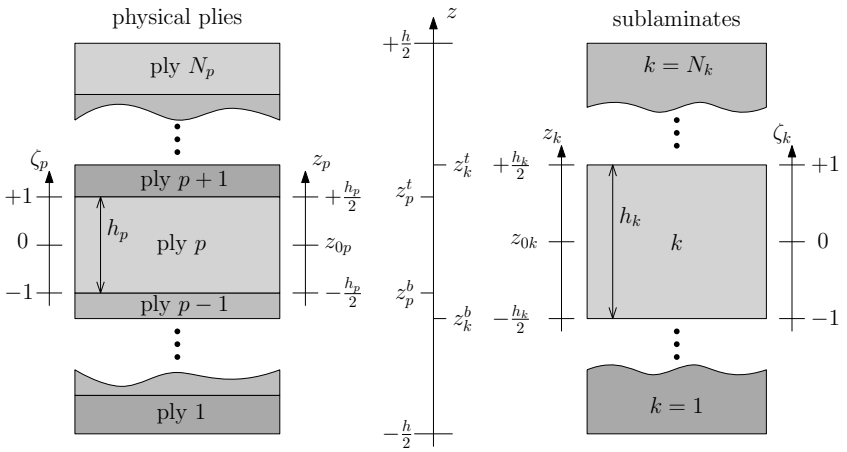

Figure 3: SGUF: geometry description and employed coordinates across the thickness.

3.2. Variable kinematics plate models in SGUF

The governing equations of displacement-based plate models shall be obtained upon introducing in axiomatic sense the through-the-thickness approximation for the kinematic field $u_i(x_\alpha, z)$ into the equilibrium statement in weak form. For a dynamic system, reference is conveniently made to Hamilton's principle and to the resulting expression:

$$\int_V \delta\epsilon_{ij}\,\sigma_{ij} + \delta u_i\,\rho\,\ddot{u}_i\;\mathrm{d}V = \int_{S_t} \delta u_i\,\bar{t}_i\;\mathrm{d}S \tag{7}$$

Tensor notation as well as summation convention over repeated indexes is adopted, with Latin indexes taking values in the set $\{1, 2, 3\}$. In Eq. (7), ϵ_{ij} and σ_{ij} represent the strain and stress tensors, respectively, ρ is the mass density, δ denotes an admissible virtual variation, and $\bar{t}_i$ is the external traction imposed at boundary region S_t. For the sake of simplicity, let $S_t = \Omega \times \pm\frac{h}{2}$, i.e., the top and bottom surfaces of the plate. Introducing the subdivision into sublaminates and upon separating the integrals over the surface Ω and the thickness h, the variational statement Eq. (7) reads

$$\sum_{k=1}^{N_k}\sum_{p=1}^{N_p^k}\int_\Omega\int_{h_p} \delta\epsilon_{ij}^{p,k}\sigma_{ij}^{p,k} + \delta u_i^{p,k}\rho^{p,k}\ddot{u}_i^{p,k}\;\mathrm{d}z\;\mathrm{d}x_1\;\mathrm{d}x_2 = \int_\Omega \delta u_i\,\bar{t}_i|_{z=\pm\frac{h}{2}}\;\mathrm{d}x_1\;\mathrm{d}x_2 \tag{8}$$

Note that Greek indexes are taken to range in $\{1, 2\}$. Limiting the scope of the proposed model within the small perturbation assumptions, the linear geometric and constitutive equations are used to define the strains and the stress, respectively, according to

$$\epsilon_{ij}^{p,k} = \frac{1}{2}\left(u_{i,j}^{p,k} + u_{j,i}^{p,k}\right); \qquad \sigma_{ij}^{p,k} = \tilde{C}_{ijlm}^{p,k}\,\epsilon_{lm}^{p,k} \tag{9}$$

where $()_{,i}$ denotes partial derivative with respect to x_i. The stiffness coefficients $\tilde{C}_{ijlm}$ are allowed to depend on the circular frequency ω according to the viscoelastic law introduced in Section 2.

Variable kinematics models are next expressed by taking advantage of the compact index notation that is characteristic of Unified Formulations. SGUF models are constructed as a LW assembly of GUF models defined in each sublaminate in terms of a polynomial expansion: the distribution of the displacement components $u_r^{p,k}$ $(r = 1, 2, 3)$ across the thickness of the p^{th} ply within the k^{th} sublaminate is postulated according to

$$u_r^{p,k}(x_1, x_2, z_p; t) = \sum_{\alpha_{u_r}=0}^{N_{u_r}^k} F_{\alpha_{u_r}}(z_p)\,\hat{u}_{\alpha_{u_r}}^{p,k}(x_1, x_2; t) \tag{10}$$

The ply-wise distributions of each individual displacement component u_r, defined by the thickness functions $F_{\alpha_{u_r}}(z_p)$, are assembled to form the sublaminate distribution according to either an ESL or an LW description. It is worth emphasising that, irrespective of the ESL or LW description adopted for the k^{th} sublaminate, the order of the polynomial expansion $N_{u_r}^k$ is unique for all the N_p^k plies and it can take different values depending on the displacement component. A constant approximation is introduced for the $u_r^{p,k}$ variable by setting $N_{u_r}^k = 0$ and $F_{\alpha_{u_r}} = 1$. The thickness functions used for defining a linear approximation ($N_{u_r}^k = 1$) are standard linear Lagrange polynomials, which interpolate the values at the top and bottom of the ply (in a LW description) or of the sublaminate (in an ESL description); this allows to enforce the perfect bond condition of adjacent plies and sublaminates through a straight-forward assembly procedure. Higher-order approximations are defined upon superposing to the linear Lagrange contributions a hierarchic enrichment defined in terms of orthogonal Legendre polynomials. Finally, an opportunely modified form of Murakami's ZigZag Function (MZZF), which vanishes at the interfaces $z_k = \left\{-\frac{h_k}{2}, \frac{h_k}{2}\right\}$, can be included within an ESL description, see also [73] for more details.

3.3. Ritz approximation

The trial solution for the displacement field along the in-plane coordinates x_α is expressed following a Ritz-type approach as

$$\hat{u}^{p,k}_{r_{\alpha_{u_r}}}(x_1, x_2; t) = \sum_{i=1}^{M} N_{u_r i}(x_1, x_2)\, U^{p,k}_{r_{\alpha_{u_r}} i}(t) \tag{11}$$

The trial functions $N_{u_r i}(x_1, x_2)$ are linearly independent and form a complete set defining an admissible solution of Eq. (7): these are built by multiplying a product of 1D orthogonal Legendre polynomials with appropriate boundary functions, which assure the exact fulfilment of the essential boundary conditions [70, 75]. Denoting by R and S the expansion's order used along x_1 and x_2, respectively, the order of the resulting 2D approximation is thus $M = RS$. It is worth emphasising that Legendre polynomials have been shown to define Ritz functions with excellent convergence and stability properties and to yield the highest degree of sparsitiy of the resulting matrices [75]. It is finally noted that the trial functions $N_{u_r i}(x_1, x_2)$ are independent of the sublaminate, and that the same order M of the Ritz expansion is used for all displacement components.

3.4. The algebraic system

The approximations across the thickness defined in Section 3.2 and the Ritz-type solution discussed in Section 3.3 are introduced into the variational statement Eq. (7). The integrals along the thickness $z \in [z_p^{\text{bot}}, z_p^{\text{top}}]$ of each ply (p) are carried out and defined in the following compact notation:

$$Z^{p\,\alpha_{u_r}\beta_{u_s}}_{(\partial)u_r\,(\partial)u_s} = \int_{z_p^{\text{bot}}}^{z_p^{\text{top}}} F_{\alpha_{u_r}(,z)} F_{\beta_{u_s}(,z)}\, \mathrm{d}z \tag{12}$$

where the index pairs (r, α) and (s, β) are used for the virtual variations and the unknown functions, respectively. An analogous compact notation is employed to denote the integrals over the reference surface Ω of the Ritz functions:

$$\mathcal{I}^{degh}_{u_r u_s\, ij} = \int_\Omega \frac{\partial^{d+e} N_{u_r i}}{\partial x_1^d\, \partial x_2^e} \frac{\partial^{g+h} N_{u_s j}}{\partial x_1^g\, \partial x_2^h}\, \mathrm{d}x_1\, \mathrm{d}x_2 \qquad (d, e, g, h = 0, 1) \tag{13}$$

The virtual variations and the unknown functions are here addressed by the index pairs (r, i) and (s, j), respectively. These invariant expressions cover all possible occurrences of the volume integrals entering the governing equations of the plate model derived from Hamilton's principle. In fact, the integral expression for the equilibrium equation given in Eq. (7) can be stated in compact

notation in the following semi-discrete form:

$$\sum_{k=1}^{N_k}\sum_{p=1}^{N_p^k} \delta U^{p,k}_{r_{\alpha_{u_r}} i}\, \tilde{C}^{p,k}_{RS}\, Z^{p\,\alpha_{u_r}\beta_{u_s}}_{(\partial)u_r(\partial)u_s}\, \mathcal{I}^{degh}_{u_r u_s ij}\, U^{p,k}_{s_{\beta_{u_s}} j}(t) + \sum_{k=1}^{N_k}\sum_{p=1}^{N_p^k} \delta U^{p,k}_{r_{\alpha_{u_r}} i}\, \rho^{p,k}\, Z^{p\,\alpha_{u_r}\beta_{u_r}}_{u_r u_r}\, \mathcal{I}^{0000}_{u_r u_r ij}\, \ddot{U}^{p,k}_{r_{\beta_{u_r}} j}(t) = \delta U^{(\mathrm{top})}_{ri}\, \mathcal{I}^{(\bar{z}_+)}_{u_r P_r i}\, P^{(\bar{z}_+)}_r(t) \;+\; \delta U^{(\mathrm{bot})}_{ri}\, \mathcal{I}^{(\bar{z}_-)}_{u_r P_r i}\, P^{(\bar{z}_-)}_r(t) \quad (14)$$

The first term represents the contribution to the stiffness matrix, in which appear the possibly frequency-dependent stiffness coefficients $\tilde{C}^{p,k}_{RS}$, with $R, S \in \{1, 2, \dots 6\}$ according to Voigt's contracted vector notation. The second term defines the contribution to the mass matrix. The right-hand side represents the work of the external distributed load $p_r(x_1, x_2, \bar{z}; t) = P^{\bar{z}}_r(t) f^{\bar{z}}_r(x_1, x_2)$ acting at $\bar{z} = \{\bar{z}_+, \bar{z}_-\} = \left\{\frac{h}{2}, -\frac{h}{2}\right\}$ along the direction r with a magnitude $\bar{P}(t)$. The load integral $\mathcal{I}^{(\bar{z})}_{u_r P_r i}$ in Eq. (14) is thus defined as

$$\mathcal{I}^{(\bar{z})}_{u_r P_r i} = \int_\Omega F_{\alpha_{u_r}}(\bar{z})\, N_{u_r i}(x_1, x_2)\; f^{\bar{z}}_r(x_1, x_2)\; \mathrm{d}x_1\, \mathrm{d}x_2 \quad (15)$$

The semi-discrete dynamic equilibrium equation Eq. (14) is next specialised to the case of a harmonic response under a temporal variation of loading amplitudes given by

$$P^{\bar{z}}_r(t) = P^{\bar{z}}_r\, \mathrm{e}^{\mathrm{i}\omega t} \quad (16)$$

Then, recalling the possibly frequency-dependent material properties of VEM, the following classical algebraic form of the governing equation Eq. (7) is finally obtained

$$\left[\boldsymbol{K}^*(\omega) - \omega^2\, \mathbf{M}\right] \boldsymbol{U}^* = \boldsymbol{F} \quad (17)$$

where $\boldsymbol{K}^*$ is the complex stiffness matrix, $\mathbf{M}$ the real mass matrix, $\boldsymbol{U}^*$ the complex generalised displacement vector and $\boldsymbol{F}$ the real amplitude vector of the total applied loads. In absence of external loading, the following nonlinear eigenvalue problem is obtained from Eq. (17):

$$\left[\boldsymbol{K}^*(\omega) - \lambda^2(\omega)\, \mathbf{M}\right] \boldsymbol{U}^* = \mathbf{0} \quad (18)$$

in which $\boldsymbol{U}^*$ defines the complex modal shapes. The complex eigenvalues take the form [48]

$$\lambda^2 = \omega^2(1 + \mathrm{i}\eta) \quad (19)$$

and define the damped eigenfrequencies $\omega = \sqrt{\mathrm{Re}(\lambda^2)}$ and the modal loss factor $\eta = \frac{\mathrm{Im}(\lambda^2)}{\mathrm{Re}(\lambda^2)}$.

3.5. Solution procedures

The SGUF-Ritz approach has been implemented in Matlab along with two solution strategies, which are basically distinguished between those treating the complex matrices and those based on the Modal Strain Energy (MSE) approach. A larger variety of solution algorithms along with a quantitative assessment of their accuracy *vs* computational time can be found in the paper by Rouleau *et al.* [21], which considers the solution of Eq. (17) on modal projection bases obtained from Eq. (18).

Linear and nonlinear eigenvalue problems. For frequency-independent VEM, Eq. (18) reduces to a linear and complex eigenvalue problem. This is solved either by the Complex Eigensolver (CE) available in Matlab, or by the classical MSE approach [16, 18], which considers a real eigenproblem and estimates the modal loss factor from the energy contributions defined by the associated real eigenmodes. For frequency-dependent VEM, the CE and MSE solution methods are implemented within an iterative scheme that employs a fixed-point iteration starting from an initial guess defined by the solution of the real eigenproblem given by $\boldsymbol{K}(0)$. The corresponding algorithms are given in Appendix A; the Iterative Complex Eigensolver (ICE) in Algorithm 1 and the Iterative Modal Strain Energy (IMSE) in Algorithm 2.

Frequency response. After discretising the frequency range of interest, the direct solution approach (Direct Frequency Response, DFR) consists in solving the linear system resulting from Eq. (17) at each value of the loading frequency. A modal projection approach is also proposed, in which the solution is obtained from the projection on a limited number of real eigenmodes defined by the MSE approach. The number of selected modes is the main parameter in this approach, depending on the frequency spectrum of interest. The interested reader is referred to the already mentioned paper by Rouleau *et al.* for other, more refined approaches for constructing reduced-order models [21].

4. Numerical results

Since the accuracy of the proposed modelling approach in the framework of elastic, undamped vibrations has been already demonstrated in [74, 75], all case studies presented in the following will be concerned with sandwich structures with embedded VEM layers. The modal loss factors of "conventional" single-core sandwich panels and for multiple-core sandwich panels are investigated in Section 4.1 and in Section 4.2, respectively. VEM with constant as well as frequency-dependent

loss factors are considered. Finally, Section 4.3 concerns the frequency response of a complex panel consisting of a triple-core sandwich panel.

4.1. Modal loss factors of sandwich plates

4.1.1. Sandwich plate with frequency-independent viscoelastic core

A first case study analyses the first 100 modes of a sandwich plate with all edges free, for which accurate numerical results were obtained by Zhang and Sainsbury by means of a conforming FEM approach [38]. The geometry of the plate and the material data are summarised in Tab. 3. The VEM core is an isotropic polymer with a constant, frequency-independent loss factor η_c. The kinematics adopted for the sandwich plate consists of a LW assembly of models with $\{N_{u_\alpha}, N_{u_3}\} = \{1, 0\}$, i.e., each ply is modelled as a Reissner-Mindlin plate with a unitary shear correction factor.

Geometric data		Material data:	elastic face	VEM core
Length	$L_1 = 348$ mm	Young's modulus	$E_f = 68.9$ GPa	$E_c = 2.67$ MPa
Width	$L_2 = 304.8$ mm	Poisson's ratio	$\nu_f = 0.3$	$\nu_c = 0.49$
Core thickness	$h_c = 0.254$ mm	Mass density	$\rho_f = 2740$ kg m^{-3}	$\rho_c = 999$ kg m^{-3}
Face thickness	$h_f = 0.762$ mm	Loss factor	$\eta_f = 0$	$\eta_c = \{0.1; 0.5; 1\}$

Table 3: Geometry and material data for the sandwich plate with frequency-independent VEM.

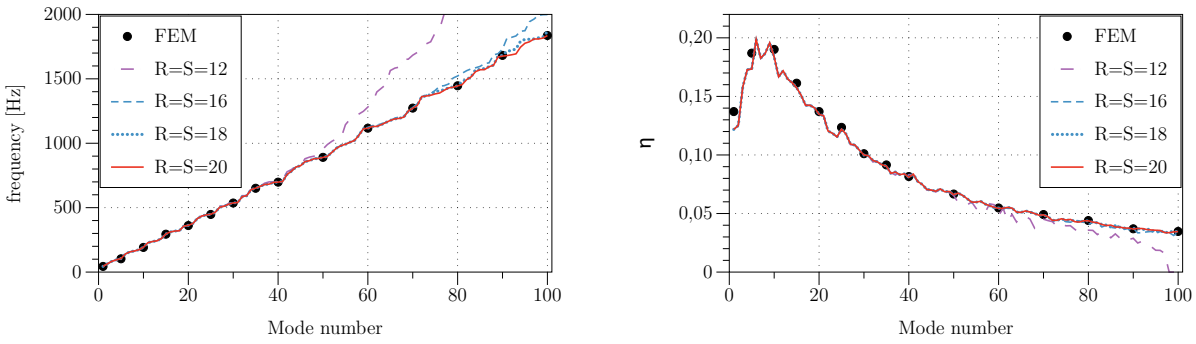

Figure 4: Modal frequencies (left) and loss factors (right) for a frequency-independent VEM with $\eta_c = 0.5$: convergence of present Ritz approach and comparison with FEM results by Zhang and Sainsbury [38].

Fig. 4 compares the eigenfrequencies and modal loss factors obtained by the present Ritz approach for the first 100 modes with those reported in [38]. These results refer to a VEM core with $\eta_c = 0.5$ and have been obtained by the Complex Eigensolver of Matlab. The results obtained with

three different orders of the Ritz expansions $R = S = \sqrt{M} = 12, 16, 20$ demonstrate the good convergence of the present method. In particular, the nonuniform distribution of the modal loss factor is well detected, with $\eta \approx 0.2$ in the range between mode 5 and mode 10 and subsequently decreasing with $\eta < 0.1$ for mode higher than 30.

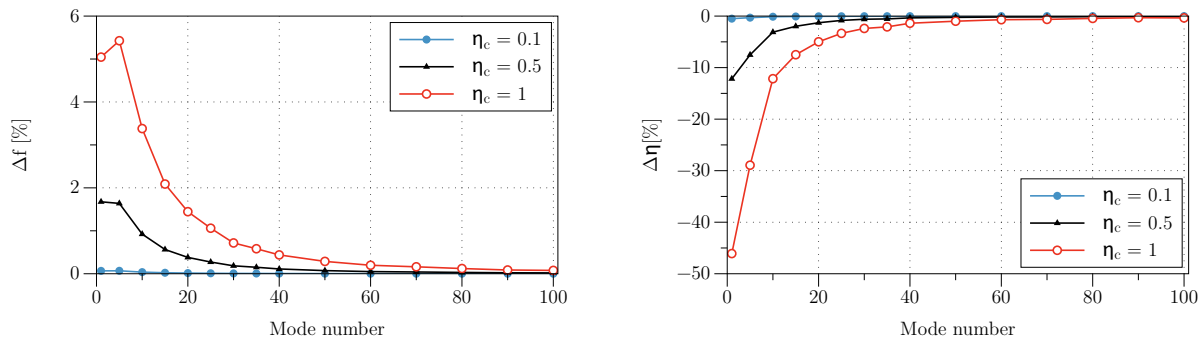

Figure 5: Percentage difference between the results of the Complex Eigensolver (CE) and the MSE approach for the eigenfrequencies (left) and modal loss factors (right) of a sandwich plate with frequency-independent VEM core.

This case study is also used to validate and assess the MSE approach. For this purpose, Fig. 5 reports the percentage difference of the MSE solution relative to the CE solution with respect to modal frequencies and loss factors: $\Delta f = \frac{f_{\mathrm{CE}} - f_{\mathrm{MSE}}}{f_{\mathrm{CE}}}$ and $\Delta\eta = \frac{\eta_{\mathrm{CE}} - \eta_{\mathrm{MSE}}}{\eta_{\mathrm{CE}}}$. The first 100 modes are considered for VEM cores with three different material loss factors, $\eta_c = 0.1, 0.5, 1$. The results show that the error introduced by the MSE approach, which disregards the complex part of the eigenmodes, is negligibly small for $\eta_c = 0.1$ but increases with the loss factor of the VEM. While the discrepancy in the frequencies remains confined below 6% even for $\eta_c = 1$, the MSE is shown to overestimate the loss factor of the fundamental mode by more than 40% and 10% for $\eta_c = 1$ and $\eta_c = 0.5$, respectively. The error is shown to decrease with the mode number because for higher modes the damping effect of the VEM becomes smaller. However, the accuracy of the Complex Eigensolver comes along a quite relevant computational effort: in fact, taking as reference the time required by the CE for solving the 100 modes, the MSE needs approximatively only half the time to compute the same 100 modes.

4.1.2. Sandwich plate with frequency-dependent viscoelastic core

This case study considers a sandwich plate whose geometry and face material are specified by the data in Tab. 3, but whose core consists of the isotropic and frequency-dependent ISD112 VEM ($\rho_c = 1600\ \mathrm{kg\,m^{-3}}$). Table 4 compares the undamped and damped eigenfrequencies and modal

loss factors obtained by the present approach against those given by Bilasse *et al.* [42] for 2 sets of boundary conditions, namely a fully clamped configuration (CCCC), and a configuration with the two edges $x_1 = (0, L_1)$ clamped and the two other edges free (CFCF). For the VEM, Bilasse *et al.* adopt the ADF-3 model as identified by Trindade *et al.* [19]. Concerning the sandwich model, Bilasse *et al.* [42] rely on CLT for the faces and FSDT for the core. Present results are computed employing the same 3-parameters ADF model as well as the FDZ model defined in Tab. 1 (ADF-5, FR2). The same plate model of the previous case study is adopted, i.e., a LW kinematics with $\{N_{u_\alpha}, N_{u_3}\} = \{1, 0\}$. Converged Ritz solutions for the first 4 modes are obtained for all configurations with $R = S = 10$. The number of parameters of the structural model is 9 and the resulting discrete system has thus 900 DOF. The damped properties (f, η_l) reported in the reference work are obtained within a "simplified approach" based on the assumption $\omega \approx \omega_0$ [42]. Therefore, in addition to the undamped eigenfrequency f_0 and the converged values (f, η) obtained at the end of the iterative procedure, Tab. 4 also reports the approximate value η_1 that is obtained after the first iteration of the fixed-point algorithm, see Appendix A.

		Ref. [42]			present ADF-3				present FDZ		
BC	Mode	f_0 [Hz]	f [Hz]	η_l	f_0 [Hz]	f [Hz]	η_1	η	f [Hz]	η_1	η
CCCC	1	76.65	83.01	0.246	76.57	83.10	0.247	0.253	83.75	0.238	0.248
	2	133.54	146.61	0.258	133.49	146.91	0.259	0.269	148.15	0.261	0.274
	3	154.04	168.92	0.257	153.52	168.76	0.257	0.269	170.32	0.260	0.273
	4	204.59	225.27	0.270	204.34	225.59	0.269	0.283	228.05	0.270	0.284
CFCF	1	44.23	46.62	0.218	44.26	46.69	0.217	0.223	47.42	0.202	0.210
	2	54.87	58.28	0.209	54.87	58.33	0.209	0.214	58.94	0.195	0.203
	3	100.52	112.25	0.238	100.43	112.28	0.242	0.248	113.05	0.238	0.247
	4	107.56	117.43	0.249	107.46	117.61	0.250	0.258	118.44	0.249	0.261

Table 4: Undamped and damped modal frequencies and loss factors for the sandwich plate with ISD112 core.

The results in Tab. 4 show that the damped eigenfrequencies f and the approximate loss factors η_1 obtained by the present SGUF-Ritz with the ADF-3 model of [19] agree very well with the values (f, η_l) reported by Bilasse *et al.* [42]. The damped properties computed upon adopting the FDZ model obtained from the ADF-5 model of [5] are also in agreement: the maximum discrepancy attributed to the different VEM model is found to be less than 6%. It should be noted that loss factors

obtained at the end of the fixed-point iteration can be quite different from those estimated from the assumption $\omega \approx \omega_0$. This means that care should be taken adopting a computationally less expensive simplified approach for solving the nonlinear eigenvalue problem of frequency-dependent VEM.

In order to evaluate the impact of the iterative procedures, the ICE and IMSE solvers are next compared. For this, the results of Tab. 4 obtained with the present FDZ model for the fully clamped panel are extended to the first 50 modes. In this case, a Ritz solution of higher order is required with $R = S = 24$, with a total number of DOF equal to 5184. Figure 6 (left) reports the damped frequencies and loss factors obtained by both solvers, while Fig. 6 (right) displays the relative percentage difference between the two solvers. The IMSE approach is seen to match well the ICE solution, with maximum discrepancies in the loss factor and eigenfrequencies that are less than 5% and 2%, respectively. Note that the loss factor of the VEM is larger than 1 for frequencies larger than 300 Hz, see Fig. 1. The accuracy of IMSE comes along with a substantially less important computational effort: for reaching the tight tolerance of $\epsilon = 10^{-6}$ for each of the 50 modes, the ICE requires 7 iterations, each involving a complex eigenvalue extraction, while the IMSE needs only 6 iterations involving only a real eigenproblem to be solved; the IMSE requires eventually only 60% of the computational time required by the ICE.

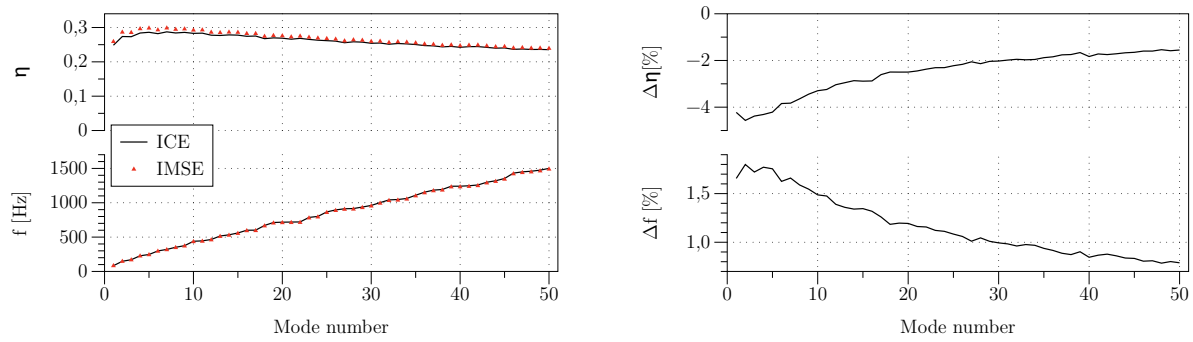

Figure 6: Sandwich plate with ISD112 core (CCCC): comparison between the ICE and IMSE solvers.

The damped dynamic structural response of the sandwich panel with ISD112 core is next considered. The panel is simply-supported (SSSS) and subjected to a harmonic point load excitation of $F = -2$ kN acting in $P(x = L_1/4, y = L_2/4)$ over the frequency range $f \in [0, 300]$ Hz. Figure 7 displays the FRF of the point P obtained with the FDZ model with a converged Ritz solution ($R = S = 14$, thus 1764 DOF). Present results obtained with the FDZ model are compared to those digitised from the graphics reported by Bilasse and Oguamanam [79], obtained with the same

ADF-3 model of [19]. Three sets of results are reported, namely the DFR and the frequency response computed by the modal projection approach labelled "RBn", where n indicates the number of real and undamped modes that span the projection basis. The results pertaining to a small basis with $n = 5$ and a rich one with $n = 150$ are given in Fig. 7. An overall reasonable agreement with the solutions provided by Bilasse and Oguamanam [79] is found: the maximum discrepancies of less than 2 [dB] are attributed to the different numerical method adopted by [79], based on FEM and ANM. It is worthwhile noticing that the accuracy of the reduced basis approach could be improved upon including the damping of the system, i.e., using complex modes instead of real modes, and upon adopting a static correction [21]. As far as the computational cost is concerned, the RB5 and RB150 take 40% and 65% of the time required for solving the DFR, respectively.

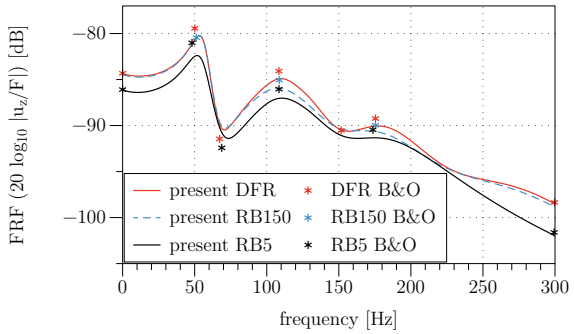

Figure 7: Frequency response function of $P(x, y) = (L_1/4, L_2/4)$ of the SSSS sandwich plate with ISD112 core: Direct Frequency Response (DFR) and FR obtained from a real basis with 5 and 150 modes.

4.2. Sandwich structures with multiple cores

The previous case studies adopted a first-order kinematics for all plies constituting the sandwich plate, and they thus allowed to validate the proposed modelling framework based on the Ritz method for viscoelastically damped structures. In the remainder of the paper, the attention will be given to the variable kinematics capabilities of the SGUF upon introducing different kinematics for the description of individual layers constituting composite plates that host multiple viscoelastic plies.

4.2.1. Double-core sandwich beam

This case study has been proposed by Lewandowski and Baum [43] and examines the first four vibration modes of a moderately thick sandwich beam of length $L_1 = 200\,\text{mm}$ and thickness $H = 11\,\text{mm}$, consisting of 3 elastic plies separated by two VEM cores. The elastic and isotropic

plies are made out of Aluminium ($E_f = 70.3\,\text{GPa}$, $\nu_f = 0.3$, $\rho_f = 2690\,\text{kg m}^{-3}$); the outer plies have a thickness of $h_1 = h_5 = 1\,\text{mm}$ and the central ply has a thickness of $h_3 = 5\,\text{mm}$. The two VEM cores have a thickness of $h_2 = h_4 = 2\,\text{mm}$ each and are made out of a frequency-dependent polymer whose behaviour is described in terms of the four-parameter FDZ model according to the data reported in Tab. 5. The VEM is isotropic with a constant Poisson's coefficient $\nu_c = 0.5$ and mass density $\rho_c = 1600\,\text{kg m}^{-3}$. Three kinds of boundary conditions are investigated with increasing degree of static indeterminacy, namely a cantilever (clamped-free), a propped (clamped-supported) and a clamped (clamped-clamped) configuration.

$E_0 = 1.5\,\text{MPa}$	$E_\infty = 69.95\,\text{MPa}$	$\alpha = 0.7915$	$\tau = 1.4052\,10^{-5}\,\text{s}$

Table 5: Parameters of the FD Zener model for the polymer used in the double-core sandwich beam.

Lewandowski and Baum employed a LW model based on CLT for the elastic plies and FSDT for the VEM plies [43]. However, the moderate slenderness of the beam and the presence of a double VEM core may require refined kinematic models for grasping the damped properties of the structure and a model assessment is, hence, proposed. Figure 8 reports the damped frequencies of the cantilever, propped and clamped beams, obtained with the present Ritz approach ($R = 10, S = 1$) and two different LW models: $\text{LD}_{1,0}$, adopts the $\{N_{u_1}, N_{u_3}\} = \{1, 0\}$ model in each ply, while LD4 is a quasi-3D model that adopts a fourth-order approximation for all displacement components ($N_{u_i} = 4$ for $i = 1, 2, 3$) in each ply. It is worth emphasising that, contrary to LD4, $\text{LD}_{1,0}$ employs the reduced stiffnesses in accordance with the plane stress assumption ($N_{u_3} = 0$). The curves reported in Fig. 8 show an excellent agreement between these two models for the 3 boundary conditions, and an overall good agreement with the results reported by Lewandowski and Baum (L&B) [43].

The modal loss factors of the cantilever, propped and clamped beams, obtained by several kinematic models, are reported in Fig. 9. In addition to the LD4 and the $\text{LD}_{1,0}$ models, two other models are considered which all keep the same $\{N_{u_1}, N_{u_3}\} = \{1, 0\}$ kinematics for the elastic plies but differ in the assumptions made for the VEM core: the $\{1, 0\}/\{3, 0\}$ model adopts a third-order expansion for the in-plane displacement ($N_{u_1} = 3$) with a constant out-of-plane deflection ($N_{u_3} = 0$), which calls for the use of the reduced plane stress constitutive law; the $\{1, 0\}/\{1, 2\}$ model adopts a $\{N_{u_1}, N_{u_3}\} = \{1, 2\}$ kinematics, which includes a linearly varying transverse normal deformation in the VEM cores and, therefore, the full 3D constitutive law. The number of parameters of the

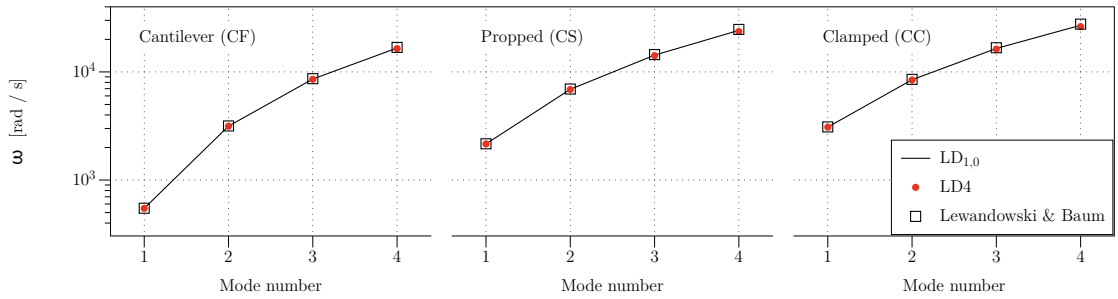

Figure 8: Double-core sandwich beam with frequency-dependent VEM: modal circular frequencies for the cantilever, propped and clamped configurations.

adopted structural models is 13 for LD$_{1,0}$, 21 for $\{1,0\}/\{3,0\}$, 17 for $\{1,0\}/\{1,2\}$ and 63 for LD4.

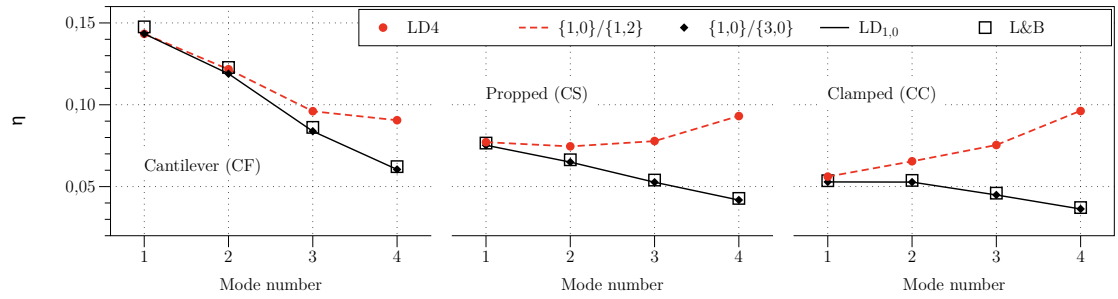

Figure 9: Double-core sandwich beam with frequency-dependent VEM: modal loss factors for the cantilever, propped and clamped configurations.

While the damped frequency appears to be rather insensitive to the kinematics employed in the LW models, Fig. 9 shows a substantially different behaviour between the models retaining the full 3D constitutive law (i.e., LD4 and $\{1,0\}/\{1,2\}$) and those relying on the plane stress assumption (i.e., L&B, LD$_{1,0}$ and $\{1,0\}/\{3,0\}$). It can be seen that the transverse normal deformation enhances the modal loss factor, this increase being more pronounced with a higher degree of hyperstaticity and for the higher modes. On the contrary, if the transverse normal deformation within the VEM cores is neglected, the modal loss factor appears to decrease with mode number and degree of hyperstaticity. These results show that transverse compressional damping can play a significant role in the modal response of sandwich structures, which thus calls for refined plate models that retain the full 3D constitutive law.

4.3. *Dynamic response of a triple-core panel*

A new case study is finally proposed that deals with the dynamic characterisation of a non-conventional, triple-core sandwich construction. The configuration is inspired from the studies for innovative solutions for helicopter cabin noise reduction, which has been the research activity of the Action Group 20 promoted by the *Garteur* consortium [80]. The panel is of moderate slenderness, with a square planform with $L_1 = L_2 = 840\,\text{mm}$ and a total thickness of $H = 21.68\,\text{mm}$. Figure 10 illustrates the composite stack made out of 13 plies: it consists of a symmetric layup of 4 plies of glass fabric (GFRP) and a nomex honeycomb core glued to a melamine foam. Ply thicknesses as well as elastic material data are reported in Tab. 6. Following the recommendations of the *Garteur* consortium, the loss factors are considered frequency-independent.

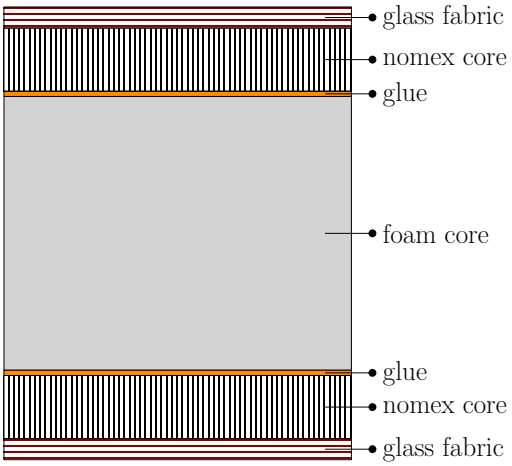

Figure 10: Sketch of triple-core sandwich stack.

Material (ply no.)	h_p [mm]	$E_1 = E_2$	E_3	ν	G_{12}	G_{13}	G_{23}	η [%]	$\rho[\frac{\text{kg}}{\text{m}^3}]$
GFRP (1–4; 10–13)	0.275	21 000	21 000	0.13	3 000	3 000	3 000	0.01	1600
Nomex (5; 9)	3	1	330	0	1	85	38	0.05	96
Glue (6; 8)	0.240	1 950	1 950	0.4	700	700	700	0.01	1050
Melamine foam (7)	13	0.5	0.23	0	0.065	0.065	0.065	0.1	11.7

Table 6: Material data and stacking sequence of the triple-core panel (moduli expressed in [MPa]).

Gorgeri *et al.* investigated the free-vibration response of the fully clamped panel and compared the numerical predictions obtained by the present Ritz-SGUF approach against experimental values [74]. Converged solutions were obtained with Ritz expansion orders $R = S = 26$ and these orders

are employed for the present analysis as well. The first 300 natural frequencies of the panel are reported in Fig. 11 for 3 different kinematic models for the melamine foam core, labelled in the following as MF$\{N_{u_\alpha}, N_{u_3}\}$: the MF{1,0} model adopts the FSDT kinematics and the reduced constitutive law, while the MF{3,2} and the MF{1,2} models retain the 3D constitutive law. The other plies are modelled as follows: the 4 GFRP plies are regrouped in 1 sublaminate with FSDT kinematics; the nomex core and glue ply form another sublaminate, for which a ply-wise FSDT model has been adopted. As a result, the SGUF models adopting the {3, 2}, the {1, 2} and the {1, 0} kinematics for the melamine foam ply have 23, 19 and 17 parameters, respectively, and their corresponding total DOF number are thus 15 548, 12 844 and 11 492, respectively. A shear correction factor of $\kappa^2 = 5/6$ has been employed for the FSDT and $\{1, 2\}$ kinematics.

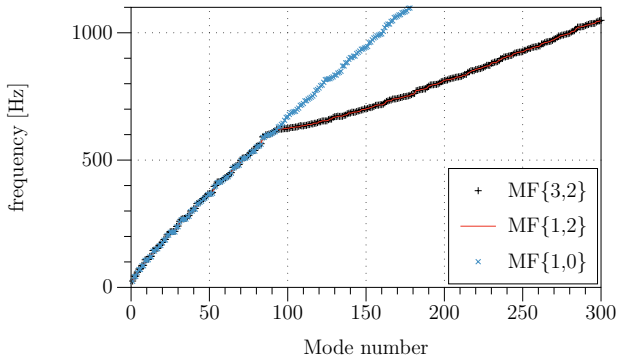

Figure 11: First 300 natural frequencies of the CCCC triple-core panel for 3 models for the melamine foam core.

The analysis in [74] showed that vibration modes with eigenfrequencies higher than 620 Hz started to involve important through-the-thickness stretch of the weak melamine foam core. This transition is characterised in Fig. 11 by an abrupt change of slope of the curve: the modal density is higher for $f > 620$ Hz, due to the presence of both long-wave thickness modes and in-plane modes with decreasing wavelengths. Figure 12 illustrates exemplarily 4 couples of modal shapes in terms of in-plane patterns and cross-sectional views, where each couple shares the same number of half-waves along the in-plane directions x and y. The first couple Fig. 12(a) and Fig. 12(b) has one half-wave in the $(x, y)-$plane and concerns the modes number 1 (25.0 Hz) and 94 (621.0 Hz); it is noted that the latter mode has a predominant through-the-thickness deformation of the melamine foam core. The subsequent modes 95, 97 and 98, reported in Fig. 12(d), Fig. 12(f) and Fig. 12(h), respectively, occur within a narrow frequency band beyond 621 Hz: these are again essentially thickness-stretch modes whose in-plane pattern is defined by a rather low number of half-waves,

just as the modes 2,4 and 5 reported in Fig. 12(c), Fig. 12(e) and Fig. 12(g), respectively.

From Fig. 11 it is evident that if FSDT kinematics is adopted for the melamine foam, then no change in the modal density occurs because no thickness modes can be captured. Furthermore, the results of MF{3,2} and MF{1,2} are barely distinguishable, a third-order shear deformation is thus not as relevant as the inclusion of the thickness stretch. Results obtained with refined kinematic models for the nomex cores have been omitted for the sake of brevity because no relevant difference has been found in the considered frequency range.

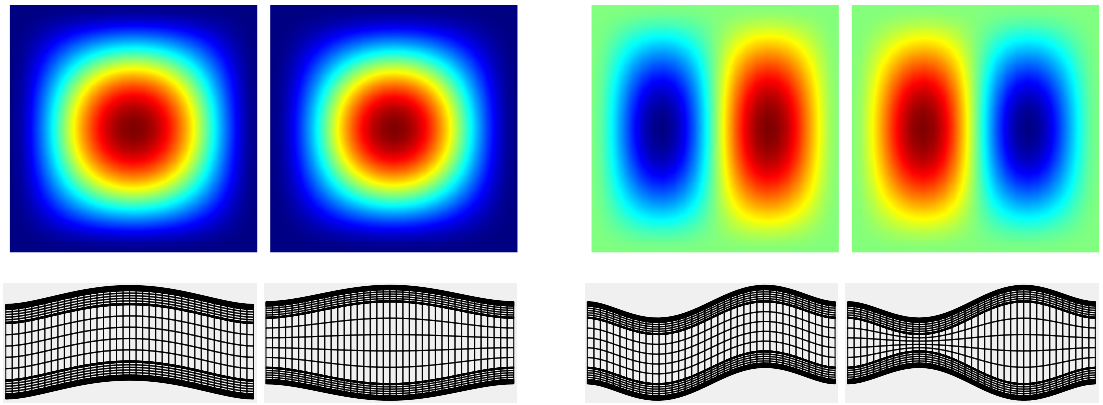

(a) Mode 1: 24.98 Hz (b) Mode 94: 621.0 Hz (c) Mode 2: 44.23 Hz (d) Mode 95: 621.7 Hz

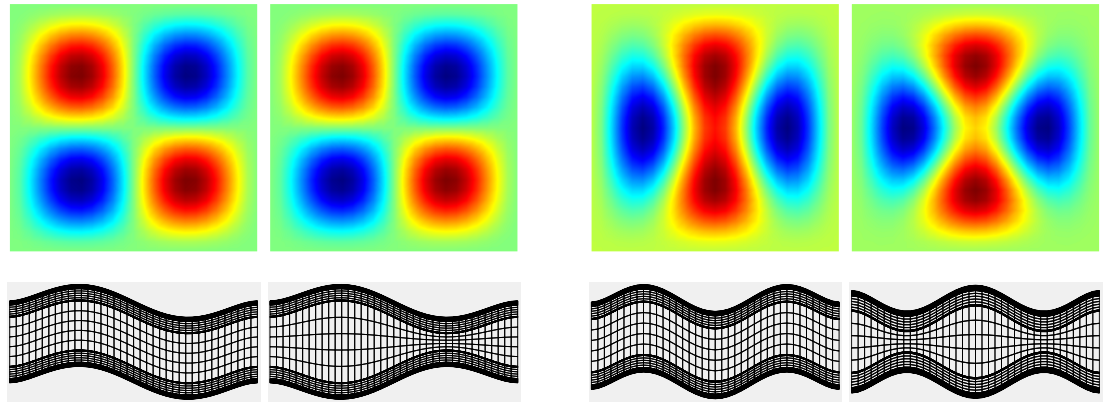

(e) Mode 4: 60.55 Hz (f) Mode 97: 622.6 Hz (g) Mode 5: 72.13 Hz (h) Mode 98: 623.6 Hz

Figure 12: Modal shapes with similar in-plane pattern but different through-the-thickness deformation.

In the following, the focus is set on the frequency response over the range $f \in [0, 600]$ Hz of the fully clamped panel excited at $P(x_1 = \frac{L_1}{4}, x_2 = \frac{L_2}{4}, z = \frac{h}{2})$ by a harmonic force of magnitude $F = -2$ kN. The DFR of point P obtained with the MF{1,2} and MF{1,0} models is given in Fig. 13 (left). A good agreement is found for $f \leq 300$ Hz: the MF{1,0} model captures well all peaks, except

for the response at $f \approx 150\,\text{Hz}$, where it predicts a lower amplitude compared to the MF{1,2} model. The discrepancies increase for higher frequencies, where MF{1,0} systematically underestimates the response. From the amplitude and phase plots corresponding to the FRF, shown in Fig. 13 (right), it appears that the main discrepancies arise in the phase diagram, i.e., due to a different representation of the viscoelastic damping of the melamine foam. One may notice the large differences at $f \approx 150\,\text{Hz}$ as well as for $f > 300\,\text{Hz}$.

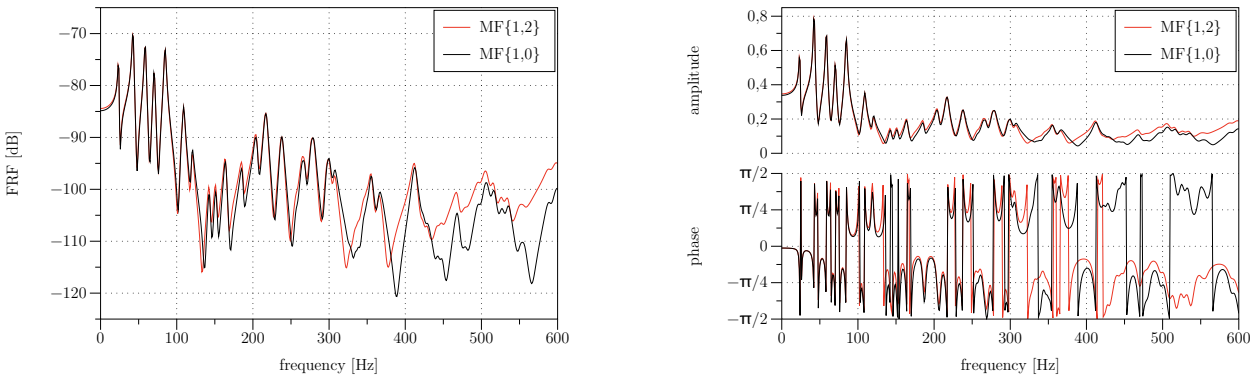

Figure 13: FRF of the triple-core panel (left) and related amplitude and phase diagrams (right): comparison of MF{1,2} and MF{1,0} models.

The DFR is next compared against the FRF obtained by means of the projection on the first n real undamped modes, with $n = \{25, 50, 100, 150\}$, see Fig. 14. From the free-vibration analysis results in Fig. 11, the eigenfrequencies f_n of the n^{th} mode are $f_{25} = 216.1\,\text{Hz}$, $f_{50} = 365.8\,\text{Hz}$, $f_{100} = 625.3\,\text{Hz}$, $f_{150} = 701.2\,\text{Hz}$. The FRF spanned by the first 25 and 50 real modes are obviously limited to the corresponding maximum frequencies. A good agreement is however found for the low frequency range $f \leq 110\,\text{Hz}$, i.e., half of the maximum frequency retained in the RB25. The RB100 and RB150 solutions yield similar FRF, with a slight accuracy increase of the RB150 in the high frequency range $f > 300\,\text{Hz}$. In this region, it is further noticed that the differences between the RB100 and RB150 are smaller if the MF{1,0} model is used for the weak and highly damping melamine foam ply. The discrepancies of the modal projection solutions with respect to the DFR are generally larger if the MF{1,2} model is used. This is attributed to the need of the truncated basis to include several thickness modes in order to represent the damping effect of the melamine foam.

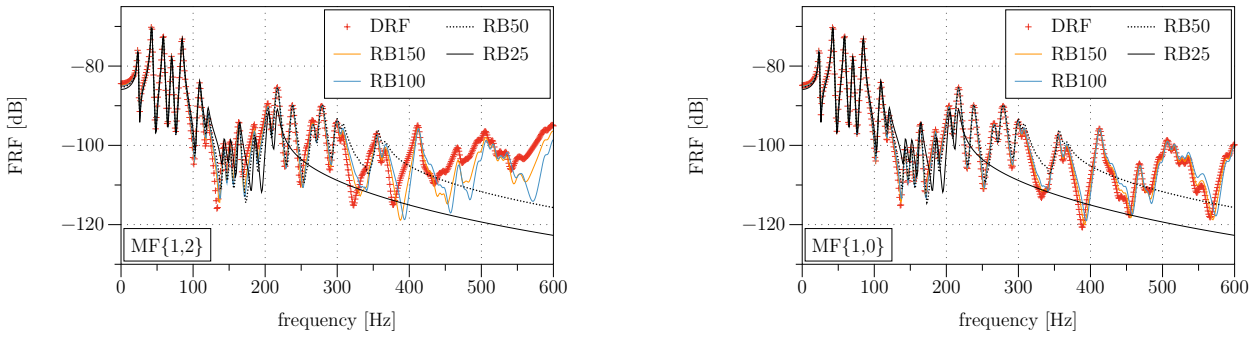

Figure 14: FRF of the triple-core panel obtained by DFR and by RBn modal projection: MF{1,2} model (left) and MF{1,0} model (right).

5. Conclusions

The paper discussed the extension of the SGUF-Ritz formulation to the dynamic response in the frequency domain of composite panels hosting viscoelastic plies. Due to the primary role played by sandwich structures in many mechanical and aerospace applications, this extension represents an important step toward the development of a numerical tool capable to analyse more realistic panel configurations, including viscoelastic layers for vibration or acoustic damping. The approach is developed in the framework of the variable kinematics SGUF formulation, and approximate solutions are retrieved by referring to an efficient Ritz method. The main advantage of the proposed strategy relies in the possibility of modelling any configuration with the desired level of detail by properly combining the definition of the sublaminates with the corresponding kinematic theories. Therefore, the structural model for sandwich panels can be tuned to the desired accuracy upon introducing dedicated assumptions for the behaviour of the stiff skins and the soft cores. In fact, classical models with few parameters and refined models requiring a larger number of parameters can be combined, in order to achieve a best compromise between accuracy and number of degrees of freedom, i.e., for optimising the computational efficiency. Moreover, the influence of specific model assumptions can be assessed in a straightforward manner, as exemplarily highlighted with respect to the $\sigma_{zz} = 0$ assumption in VEM cores. Special attention has been paid to the description of the frequency-dependent viscoelastic behaviour, for which a fractional derivatives Zener-type model has been implemented along with more conventional models relying on series expansions. Different solution procedures for the complex eigenvalue problem have been also prototypically implemented. The quality of the predictions is demonstrated by comparison with available solutions

for different panels, demonstrating that quasi-3D accuracy can be achieved with a relatively small number of degrees of freedom, much less with respect to those required by a purely LW approach. Conventional single-core sandwich plates as well complex multi-core panels can be investigated, irrespective of the thickness and of the boundary conditions.

Further work shall address the extension to curved panels, the evaluation of acoustic properties and the optimisation of viscoelastic composite panels. In order to quantitively assess the accuracy and, hence, the efficiency of the various structural kinematics, it could be useful to introduce an error measure accounting for the strain and kinetic energy contributions that define the dynamic response of the sandwich panel. The computational efficiency of the approach could be also further improved upon adopting enhanced reduced-order modelling techniques. Finally, it is worthwhile mentioning that the modal response or the direct FRF obtained by efficient computational tools like the present one could be advantageously used within inverse identification techniques for characterising the frequency-dependent damping properties of the sandwich plate; this would allow to take into account the alteration of the bare VEM properties induced by the process for manufacturing the composite structure.

Acknowledgments

Riccardo Vescovini and Lorenzo Dozio would like to thank Ministero dell'Istruzione, dell'Università e della Ricerca for funding this research under PRIN 2017 program.

Appendix A. Solution algorithms

Algorithm 1 The ICE algorithm for N modes

1: solve Eq. (18) with $\omega = 0$: compute $\lambda(0)$ ▷ Initial guess: N real eigenvalues
2: **for** $j = 1 : N$ **do**
3: Initialise the error $\epsilon = 1$ and the eigenfrequency $\tilde{\omega} = \lambda_j(0)$
4: **while** $\epsilon > \epsilon_{tol}$ **do** ▷ used tolerance: $\epsilon_{tol} = 1e^{-6}$
5: solve $\left[\boldsymbol{K}^*(\tilde{\omega}) - \lambda^2(\tilde{\omega})\boldsymbol{M}\right]\boldsymbol{U} = \boldsymbol{0}$
6: compute the error: $\epsilon = \frac{\tilde{\omega} - \sqrt{\mathrm{Re}(\lambda_j^2(\tilde{\omega}))}}{\sqrt{\mathrm{Re}(\lambda_j^2(\tilde{\omega}))}}$
7: update the eigenfrequency: $\tilde{\omega} = \sqrt{\mathrm{Re}(\lambda_j^2(\tilde{\omega}))}$
8: **end while**
9: $\omega_j = \tilde{\omega};\ \eta_j = \frac{\mathrm{Im}(\lambda_j^2)}{\mathrm{Re}(\lambda_j^2)}$ ▷ converged solution: damped eigenfrequencies & modal loss factor
10: **end for**

Algorithm 2 The IMSE algorithm for N modes

1: solve Eq. (18) with $\omega = 0$: compute $\lambda(0)$ ▷ Initial guess: N real eigenvalues
2: **for** $j = 1 : N$ **do**
3: Initialise the error $\epsilon = 1$ and the eigenfrequency $\tilde{\omega} = \lambda_j(0)$
4: **while** $\epsilon > \epsilon_{tol}$ **do** ▷ used tolerance: $\epsilon_{tol} = 1e^{-6}$
5: solve $\left[\mathrm{Re}(\boldsymbol{K}^*(\tilde{\omega})) - \lambda^2(\tilde{\omega})\boldsymbol{M}\right]\boldsymbol{U} = \boldsymbol{0}$
6: compute the error: $\epsilon = \frac{\tilde{\omega} - \lambda_j(\tilde{\omega})}{\lambda_j(\tilde{\omega})}$
7: update the eigenfrequency and modal shapes: $\tilde{\omega} = \lambda_j(\tilde{\omega});\ \boldsymbol{U}_j = \boldsymbol{U}_j(\tilde{\omega})$
8: **end while**
9: $\omega_j = \tilde{\omega};\ \eta_j = \frac{\boldsymbol{U}_j^T\,\mathrm{Im}\left(\boldsymbol{K}(\omega_j)\right)\boldsymbol{U}_j}{\boldsymbol{U}_j^T\,\mathrm{Re}\left(\boldsymbol{K}(\omega_j)\right)\boldsymbol{U}_j}$ ▷ converged solution: damped eigenfrequencies & modal loss factor
10: **end for**

References

[1] M. D. Rao, Recent applications of viscoelastic damping for noise control in automobiles and commercial airplanes, J. Sound Vibr. 262 (2003) 457–474.

[2] A. M. Baz, Active and Passive Vibration Damping, John Wiley & Sons, Ltd, 2019.

[3] D. I. G. Jones, On the temperature-frequency analysis of polymer dynamic mechanical behaviour, J. Sound Vibr. 140 (1990) 85–102.

[4] D. J. McTavish, P. C. Hughes, Modeling of linear viscoelastic space structures, J. Vibr. Acoust. 115 (1993) 103–110.

[5] G. A. Lesieutre, E. Bianchini, Time domain modeling of linear viscoelasticity using anelastic displacement fields, J. Vibr. Acoust. 117 (1995) 424–430.

[6] R. L. Bagley, P. J. Torvik, A theoretical basis of the application of fractional calculus to viscoelasticity, J. Rheol. 27 (3) (1983) 201–210.

[7] R. Koeller, Applications of fractional calculus to the theory of viscoelasticity, J. Appl. Mech. 51 (12) (1984) 299–307.

[8] R. L. Bagley, P. J. Torvik, On the fractional calculus model of viscoelastic behavior, J. Rheol. 30 (3) (1986) 133–155.

[9] T. Pritz, Analysis of four-parameter fractional derivative model of real solid materials, J. Sound Vibr. 195 (1996) 103–115.

[10] T. Pritz, Five-parameter fractional derivative model for polymeric damping materials, J. Sound Vibr. 265 (2003) 935–952.

[11] A. C. Galucio, J.-F. Deü, R. Ohayon, Finite element formulation of viscoelastic sandwich beams using fractional derivative operators, Comput. Mech. 33 (2004) 282–291.

[12] H. Voss, An Arnoldi method for nonlinear eigenvalue problems, BIT Numer. Math. 44 (2004) 387–401.

[13] X. Chen, H. L. Chen, X. L. Hu, Damping predication of sandwich structures by order-reduction-iteration approach, J. Sound Vibr. 222 (1999) 803–812.

[14] B.-A. Ma, J.-F. He, A finite element analysis of viscoelastically damped sandwich plates, J. Sound Vibr. 152 (1992) 107–123.

[15] E. M. Daya, M. Potier-Ferry, A numerical method for nonlinear eigenvalue problems application to vibrations of viscoelastic structures, Comput. Struct. 79 (2001) 533–541.

[16] M. L. Soni, Finite element analysis of viscoelastically damped sandwich structures, in: The Shock and Vibration Bulletin, Vol. 51 (Pt 1), The Shock and Vibration Information Center, 1981, pp. 97–109.

[17] E. E. Ungar, E. M. Kerwin, Jr., Loss factors of viscoelastic systems in terms of energy concepts, J. Acoust. Soc. Am. 34 (7) (1962) 954–957.

[18] C. D. Johnson, D. A. Kienholz, Finite element prediction of damping in structures with constrained viscoelastic layers, AIAA J. 20 (1982) 1284–1290.

[19] M. A. Trindade, A. Benjeddou, R. Ohayon, Modeling of frequency-dependent viscoelastic materials for active-passive vibration damping, J. Vibr. Acoust. 122 (2000) 169–174.

[20] R. A. S. Moreira, J. Dias Rodrigues, Multilayer damping treatments: modeling and experimental assessment, J. Sandwich Struct. Mater. 12 (2010) 181–198.

[21] L. Rouleau, J.-F. Deü, A. Legay, A comparison of model reduction techniques based on modal projection for structures with frequency-dependent damping, Mech. Syst. Signal Pr. 90 (2017) 110–125.

[22] E. M. Kerwin, Jr., Damping of flexural waves by a constrained viscoelastic layer, J. Acoust. Soc. Am. 31 (7) (1959) 952–962.

[23] B. E. Douglas, J. C. S. Yang, Transverse compressional damping in the vibratory response of elastic-viscoelastic-elastic beams, AIAA J. 16 (1978) 925–930.

[24] C. M. A. Vasques, L. C. Cardoso, Viscoelastic damping technologies: Finite element modeling and application to circular saw blades, in: C. M. A. Vasques, J. Dias Rodrigues (Eds.), Vibration and Structural Acoustics Analysis, Springer Science+Business Media B. V., 2011, Ch. 9, pp. 207–264.

[25] L. Rouleau, A. Legay, J.-F. Deü, Interface finite elements for the modelling of constrained viscoelastic layers, Compos. Struct. 204 (2018) 847–854.

[26] F. Kpeky, H. Boudaoud, F. Abed-Meraim, E. M. Daya, Modeling of viscoelastic sandwich beams using solid–shell finite elements, Compos. Struct. 133 (2015) 105–116.

[27] E. Carrera, Theories and finite elements for multilayered, anisotropic, composite plates and shells, Arch. Comput. Meth. Eng. 9 (2002) 87–140.

[28] J. N. Reddy, Mechanics of Laminated Composite Plates and Shells: Theory and Analysis, 2nd Edition, CRC Press, 2004.

[29] M. D'Ottavio, O. Polit, Classical, first order, and advanced theories, in: H. Abramovich (Ed.), Stability and Vibration of Thin-Walled Composite Structures, Composites Science and Engineering, Woodhead Publishing, 2017, Ch. 3, pp. 91–140.

[30] E. Carrera, Historical review of zig-zag theories for multilayered plates and shells, Appl. Mech. Rev. 56 (2003) 287–308.

[31] A. Loredo, M. D'Ottavio, P. Vidal, O. Polit, A family of of higher-order single layer plate models meeting C_z^0-requirements for arbitrary laminates, Compos. Struct. 225 (2019) 111146.

[32] R. M. J. Groh and P. M. Weaver, On displacement-based and mixed-variational equivalent single layer theories for modelling highly heterogeneous laminated beams, Int. J. Solids Struct. 59 (2015) 147–170.

[33] H. Hu, S. Belouettar, M. Potier-Ferry, E. M. Daya, Review and assessment of various theories for modeling sandwich composites, Compos. Struct. 84 (2008) 282–292.

[34] E. Carrera, S. Brischetto, A survey with numerical assessment of classical and refined theories for the analysis of sandwich plates, Appl. Mech. Rev. 62 (2009) 1–17.

[35] R. A. DiTaranto, Theory of vibratory bending for elastic and viscoelastic layered finite-length beams, J. Appl. Mech. 32 (1965) 881–886.

[36] D. J. Mead, S. Markus, The forced vibration of a three-layer, damped sandwich beam with arbitrary boundary conditions, J. Sound Vibr. 10 (1969) 163–175.

[37] J.-F. He, B.-A. Ma, Analysis of flexural vibration of viscoelastically damped sandwich plates, J. Sound Vibr. 126 (1988) 37–47.

[38] Q. J. Zhang, M. G. Sainsbury, The Galerkin element method applied to the vibration of rectangular damped sandwich plates, Comput. Struct. 74 (2000) 717–730.

[39] A. Fasana, S. Marchesiello, Rayleigh-Ritz analysis of sandwich beams, J. Sound Vibr. 241 (2001) 643–652.

[40] M. D. Rao, S. He, Dynamic analysis and design of laminated composite beams with multiple damping layers, AIAA J. 31 (1993) 736–745.

[41] J. S. Moita, A. L. Araújo, P. Martins, C. M. Mota Soares, C. A. Mota Soares, A finite element model for the analysis of viscoelastic sandwich structures, Comput. Struct. 89 (2011) 1874–1881.

[42] M. Bilasse, L. Azrar, E. M. Daya, Complex modes based numerical analysis of viscoelastic sandwich plates vibrations, Comput. Struct. 89 (2011) 539–555.

[43] R. Lewandowski, M. Baum, Dynamic characteristics of multilayered beams with viscoelastic layers described by the fractional Zener model, Arch. Appl. Mech. 85 (2015) 1793–1814.

[44] K. Akoussan, H. Boudaoud, E. M. Daya, Y. Koutsawa, E. Carrera, Sensitivity analysis of the damping properties of viscoelastic composite structures according to the layers thicknesses, Compos. Struct. 149 (2016) 11–25.

[45] W. Larbi, J.-F. Deü, R. Ohayon, Vibroacoustic analysis of double-wall sandwich panels with viscoelastic core, Comput. Struct. 174 (2016) 92–103.

[46] S. Ren, G. Zhao, A four-node quadrilateral element for vibration and damping analysis of sandwich plates with viscoelastic core, J. Sandwich Struct. Mater. 21 (2019) 1072–1118.

[47] P. Cupiał, J. Nizioł, Vibration and damping analysis of a three-layered composite plate with viscoelastic mid-layer, J. Sound Vibr. 183 (1995) 99–114.

[48] R. Rikards, A. Chate, E. Barkanov, Finite element analysis of damping the vibrations of laminated composites, Comput. Struct. 47 (1993) 1005–1015.

[49] R. A. S. Moreira, J. Dias Rodrigues, A. J. M. Ferreira, A generalized layerwise finite element for multi-layer damping treatments, Comput. Mech. 37 (2006) 426–444.

[50] Z. Huang, Z. Qin, F. Chu, Vibration and damping characteristics of sandwich plates with viscoelastic core, J. Vibr. Control 22 (2016) 1876–1888.

[51] A. L. Araújo, C. M. Mota Soares, C. A. Mota Soares, J. Herskovits, Optimal design and parameter estimation of frequency dependent viscoelastic laminated sandwich composite plates, Compos. Struct. 92 (2010) 2321–2327.

[52] J. S. Moita, A. L. Araújo, C. M. Mota Soares, C. A. Mota Soares, Finite element model for damping optimization of viscoelastic sandwich structures, Adv. Eng. Software 66 (2013) 34–39.

[53] T. S. Plagianakos, D. A. Saravanos, High-order layerwise finite element for the damped free-vibration response of thick composite and sandwich composite plates, Int. J. Numer. Meth. Eng. 77 (2009) 1593–1626.

[54] A. Bhimaraddi, Sandwich beam theory and the analysis of constrained layer damping, J. Sound Vibr. 179 (1995) 591–602.

[55] M. Ganapathi, B. P. Patel, P. Boisse, O. Polit, Flexural loss factors of sandwich and laminated composite beams using linear and nonlinear dynamic analysis, Compos. B 30 (1999) 245–256.

[56] A. Treviso, D. Mundo, M. Tournour, A C^0-continuous RZT beam element for the damped response of laminated structures, Compos. Struct. 131 (2015) 987–994.

[57] J.-W. Han, J.-S. Kim, M. Cho, Improved finite element viscoelastic analysis of laminated structures via the enhanced first-order shear deformation theory, Compos. Struct. 180 (2017) 360–377.

[58] A. Castel, A. Loredo, A. El Hafidi, B. Martin, Complex power distribution analysis in plates covered with passive constrained layer damping patches, J. Sound Vibr. 331 (2012) 2485–2498.

[59] Z. Xie, W. S. Shepard, Jr, Analytical modeling and analysis of a constrained layer damped plate to examine the impact of the transverse compressional damping component, Mech. Adv. Mater. Struct. 21 (2014) 669–679.

[60] S. Ren, G. Zhao, S. Zhang, A layerwise finite element formulation for vibration and damping analysis of sandwich plate with moderately thick viscoelastic core, Mech. Adv. Mater. Struct. (2019). DOI: 10.1080/15376494.2018.1504360.

[61] M. Cinefra, E. Carrera, A. Lamberti, M. Petrolo, Best theory diagrams for multilayered plates considering multifield analysis, J. Intellig. Mat. Sys. Struct. 28 (2017) 2184–2205.

[62] E. Carrera, M. Cinefra, M. Petrolo, E. Zappino, Finite Element Analysis of Structures through Unified Formulation, John Wiley & Sons, Ltd, Chichester, UK, 2014.

[63] L. Demasi, Partially Layer Wise advanced Zig Zag and HSDT models based on the Generalized Unified Formulation, Eng. Struct. 53 (2013) 63–91.

[64] M. D'Ottavio, A Sublaminate Generalized Unified Formulation for the analysis of composite structures and its application to sandwich plates bending, Compos. Struct. 142 (2016) 187–199.

[65] A. J. M. Ferreira, A. L. Araújo, A. M. A. Neves, J. D. Rodrigues, E. Carrera, M. Cinefra, C. M. Mota Soares, A finite element model using a unified formulation for the analysis of viscoelastic sandwich laminates, Compos. B 45 (2013) 1258–1264.

[66] B. Liu, L. Zhao, A. J. M. Ferreira, Y. F. Xing, A. M. A. Neves, J. Wang, Analysis of viscoelastic sandwich laminates using a unified formulation and a differential quadrature hierarchical finite element method, Compos. B 110 (2017) 185–192.

[67] M. Filippi, E. Carrera, Various refined theories applied to damped viscoelastic beams and circular rings, Acta Mech. 228 (2017) 4235–4248.

[68] M. Filippi, E. Carrera, S. Valvano, Analysis of multilayered structures embedding viscoelastic layers by higher-order, and zig-zag plate elements, Compos. B 154 (2018) 77–89.

[69] A. Alaimo, C. Orlando, S. Valvano, Analytical frequency response solution for composite plates embedding viscoelastic layers, Aero. Sci. Tech. 92 (2019) 429–445.

[70] L. Dozio, E. Carrera, Ritz analysis of vibrating rectangular and skew multilayered plates based on advanced variable-kinematics models, Compos. Struct. 94 (2012) 2118–2128.

[71] M. D'Ottavio, L. Dozio, R. Vescovini, O. Polit, Bending analysis of composite laminated and sandwich structures using sublaminate variable-kinematic Ritz models, Compos. Struct. 155 (2016) 45–62.

[72] R. Vescovini, M. D'Ottavio, L. Dozio, O. Polit, Buckling and wrinkling of anisotropic sandwich plates, Int. J. Engng. Sci. 130 (2018) 136–156.

[73] M. D'Ottavio, L. Dozio, R. Vescovini, O. Polit, The Ritz – Sublaminate Generalized Unified Formulation approach for piezoelectric composite plates, Int. J. Smart Nano Mater. 9 (2018) 1–22.

[74] A. Gorgeri, R. Vescovini, L. Dozio, Analysis of multiple-core sandwich cylindrical shells using a sublaminate formulation, Compos. Struct. 225 (2019) 111067.

[75] R. Vescovini, L. Dozio, M. D'Ottavio, O. Polit, On the application of the Ritz method to free vibration and buckling analysis of highly anisotropic plates, Compos. Struct. 192 (2018) 460–474.

[76] L. Rouleau, Modélisation vibro-acoustique de structures sandwich munies de matériaux viscoélastiques [*Vibro-acoustic modeling of sandwich structures with viscoelastic materials*], Ph.D. thesis, Conservatoire National des Arts et Métiers (2013).
URL https://tel.archives-ouvertes.fr/tel-00957457

[77] L. Rouleau, J.-F. Deü, A. Legay, J.-F. Sigrist, P. Marin-Courtoud, Reduced order model for noise and vibration attenuation of water immersed viscoelastic sandwich structures, in: Proceedings of Acoustics2012, Nantes, France, 2012, pp. 733–738.

[78] J. Kennedy, R. Eberhart, Particle swarm optimization, in: Proceedings of ICNN'95 – International Conference on Neural Networks, Vol. 4, IEEE, 1995, pp. 1942–1948.

[79] M. Bilasse, D. C. D. Oguamanam, Forced harmonic response of sandwich plates with viscoelastic core using reduced-order model, Compos. Struct. 105 (2013) 311–318.

[80] F. Simon, T. Haase, O. Unruh, G. Ghiringhelli, A. Parrinello, R. Vescovini, Benchmark for modelization of acoustic transmission loss applied to helicopter trim panels, in: 42nd European Rotorcraft Forum (ERF 2016), Lille, France, 2016.